

# THE INVERSE-SQUARE GAMMA-IRRADIATION ANOMALY OF THE NUCLEAR ENTERPRISES 2575 LARGE-VOLUME IONISATION CHAMBER

Alex F. Bielajew<sup>1,\*</sup>, Frédéric Tessier<sup>2</sup> and Islam El Gamal<sup>2</sup>

<sup>1</sup>Department of Nuclear Engineering and Radiological Sciences, The University of Michigan, 2355 Bonisteel Boulevard, Ann Arbor, MI 48109, USA

<sup>2</sup>Ionizing Radiation Standards, National Research Council of Canada, Ottawa, ON, Canada K1A 0R6

\*Corresponding author. bielajew@umich.edu

Received 14 July 2014; revised 4 September 2014; accepted 6 September 2014

**The Nuclear Enterprises (Model 2575) 600 cc ionisation chamber is examined to discover the cause of its anomalous behaviour in inverse-square stability measurements. Measurements and Monte Carlo calculations are employed to isolate the cause of the discrepancy. It is found that most of the effect is due to the long photon attenuation pathlengths in the long side wall of the instrument. A phenomenological procedure, based on measurements, is proposed to correct for the anomaly. The procedure results in inverse-square stability to within 0.5 % over a range of 1–7 m.**

## INTRODUCTION

Inverse-square ionisation chamber measurements involve the determination of ionisation response vs. distance, and multiplying the charge collected (for equal collection times) by  $d^2$ , where  $d$  is the distance from the centre of the source, to the centre of the sensitive volume of the chamber. If multiple chambers are employed in the measurements, and each data set is normalised at a standard distance (typically 1 m), then it is commonly expected that the individual data sets should fall on similar curves that are close to unity, with small differences that are particular to the radiation quality, and differences in instrument construction.

If the chambers are irradiated by photon beams, and the data are acquired in a large laboratory for which the scatter from the surroundings is small, and the chambers respond similarly to all photon energies, then the individual data curves should exhibit a gentle fall-off with distance, after multiplication by  $d^2$ . That gentle fall-off can be ascribed to photon attenuation in the air between the chamber and the source, and the attenuation in the measurement devices themselves.

Although it appears to be common knowledge that the Nuclear Enterprises (Model 2575) 600 cc ionisation chamber (NE2575) has an anomalous response, there is no mention of this in the refereed literature. However, at the time of this writing, a description of the effect has been reported on-line (P. Burgess (2010), *Inverse square law and problems with the NE 600 cc ion chamber*; [www.npl.co.uk/upload/pdf/20101117\\_irmf\\_burgess.pdf](http://www.npl.co.uk/upload/pdf/20101117_irmf_burgess.pdf)), ascribing the anomaly to the anisotropic angular response of this particular chamber.

The National Research Council of Canada's (NRCC) Ionizing Radiation Standards section has

been maintaining data on the NE2575 since 1996, but the anomaly has remained unexplained.

To execute this study, measurements were performed with two instruments, and the data analysed with mathematical and Monte Carlo modelling of the source, the irradiator, the ionisation chambers and the laboratory, to isolate the cause.

## EXPERIMENTAL APPARATUS

An Atlan-tech model GC 60 beam calibrator was used here for the irradiations. Some details of the Atlan-tech irradiator employed in this study were described by Shortt *et al.*<sup>(1)</sup>. The irradiator currently holds four different sources in a carousel at the centre of the unit. Compressed air is used to transfer the selected source to the collimator opening. A conical collimator is used to define a field of diameter 40 cm (i.e. the air kerma falls to 50 % of the central value at a distance of 40 cm) at 1 m<sup>(1)</sup>. (The negative gradient in flux over the lateral extent of the chamber is at most ~0.2 %, and this decrease is accounted for by taking measurement ratios of two chambers that have similar lateral extent.) When the source is exposed, an optical sensor is activated, starting the exposure timer.

An Amersham 100 Ci <sup>137</sup>Cs encapsulated source (model number CDC.711 m) was used for all irradiations. The radionuclide is present as a ceramic <sup>137</sup>Cs pellet within two layers of welded stainless steel, shown in Figure 1.

All experiments were conducted at NRCC's low-scatter laboratory, depicted in Figure 2.

A rail system extends over the low-mass aluminium-mesh floor, depicted as a hatched area in Figure 2.

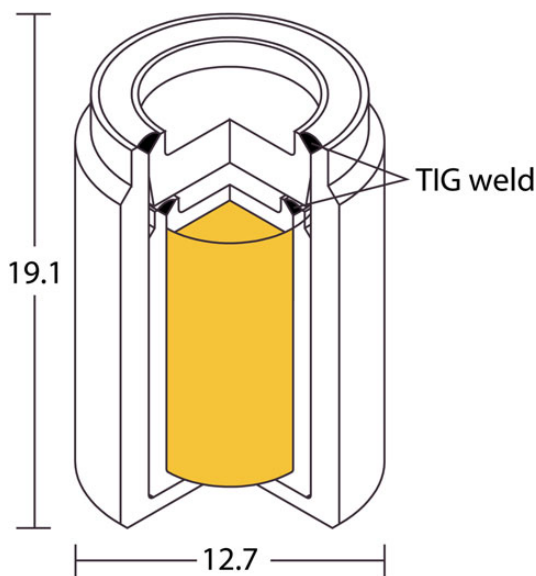


Figure 1. The doubly encapsulated stainless steel Amersham  $^{137}\text{Cs}$  source (model number CDC.711 m). All dimensions are in millimetre. The  $^{137}\text{Cs}$  ceramic pellet is the innermost cylinder in the figure. (See the user manual.)

A table can be mounted and moved on the rail system allowing its position to be reproduced to within 0.5 mm. The ionisation chambers were attached to the table, and the rail system used to translate the chamber away from the source. To determine the reference position of 1 m from the source centre to the chamber cavity centre to within 0.1 mm, a precision pointer was mounted to the front of the irradiator.

Experiments were conducted using two chambers: the NE2575, shown in Figure 3, and the Exradin A6 800 cc ionisation chamber (A6), shown in Figure 4. The A6 is composed of Shonka C-552 air-equivalent plastic, while the stem is made of Delrin. The NE2575 has a nominal active volume of 602 cc and a sensitive window area of  $100\text{ cm}^2$ .

Irradiations of the NE2575 were conducted with an additional clear perspex window attached to the chamber window with  $620\text{ mg cm}^{-2}$  thickness. The chamber base and walls are made of synthetic-resin bonded paper (SRBP), while the central electrode is made of Nylon 66. The chamber window is made of aluminised Mylar and the collecting electrode is composed of Lucite. All the surfaces inside the chamber's active volume are coated with conducting graphite (from the user manual, and confirmed during disassembly).

The chambers were mounted to a table on the rail system and the starting position was set using the 1 m reference pointer, such that the distance between the centre of the chamber cavity and the source centre

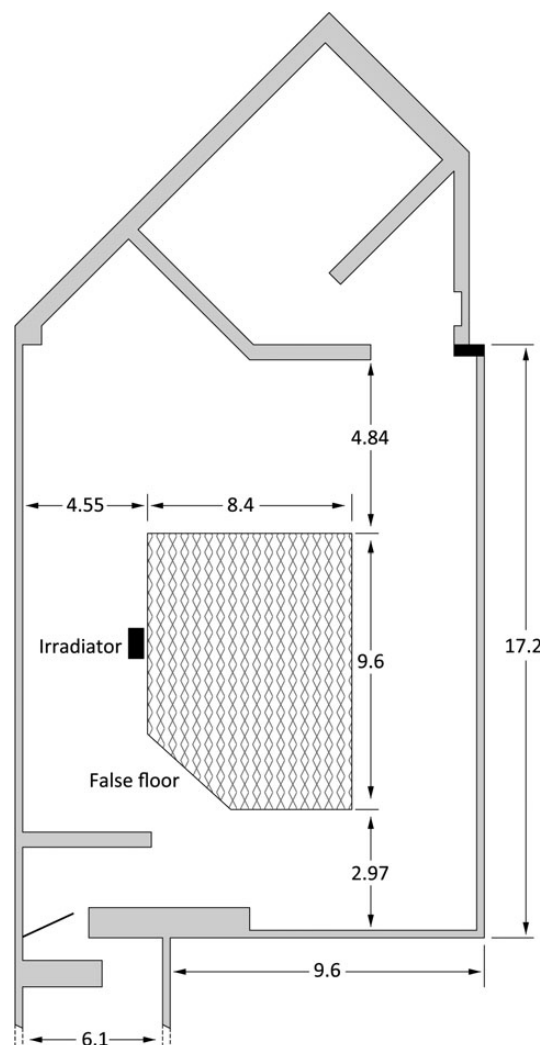


Figure 2. NRCC's low-scatter laboratory schematic (floor plan). All dimensions are given in metre. The ceiling is 7 m high. The aluminium low-mass floor shown is 4 m above an empty room below the laboratory.

was  $1.000 \pm 0.001\text{ m}$ . The rail system was then used to translate the table and the chamber away from the source with the rail system's scale allowing the position of the chamber centre to be determined relative to the starting position to within 0.5 mm.

The measurement procedure was the same for both chambers. At each position, the integration time was  $60.000 \pm 0.010\text{ s}$  and the charge was collected using a Keithley 35617 electrometer. At least five measurements were acquired and the typical standard uncertainty on each data set was 0.11 %. All measurements were corrected to standard temperature and pressure,

## INVERSE-SQUARE ANOMALY OF THE NE2575 ION CHAMBER

and the whole procedure was repeated to determine positioning repeatability and/or chamber drift. The average overall standard uncertainty on the ratio of chamber readings (NE2575/A6) is estimated to be 0.32 %.

### THE INVERSE-SQUARE MEASUREMENT DATA

Figure 5 presents both the A6 and the NE2575 data, normalised at the 1 m point and multiplied by  $d^2$ . In an ideal scenario, namely a point source irradiating a point detector in infinite vacuum, no departure from



Figure 3. Disassembled NE2575. When irradiating the chamber, the central electrode should be pointed directly towards the source. The thickness of the rear wall (not shown) is 1.5 cm. The outer cylindrical radius of the chamber is 6.255 cm.

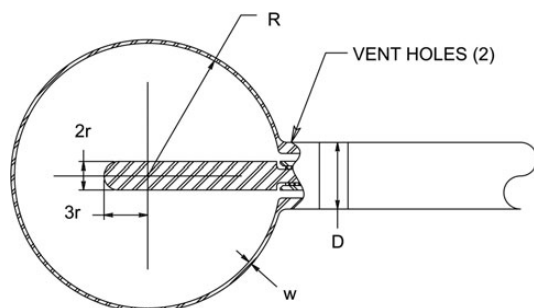


Figure 4. Exradin A6 ionisation chamber, reference #92716. Wall thickness = 0.3 cm, stem diameter = 2.22 cm, inner radius ( $R$ ) = 5.72 cm, radius of electron tip ( $r$ ) = 0.58 cm. (See the user manual.)

unity would be observed<sup>(2)</sup>. The discrepancy is due to many factors, enumerated in Table 1, and discussed in the 'ANALYSIS' section.

The A6 data clearly show a characteristic exponential fall-off at shorter distances, due to primary photon attenuation. The behaviour at larger distances is more complex, combining air attenuation and scatter from the structures of the low-scatter laboratory. This is discussed fully below.

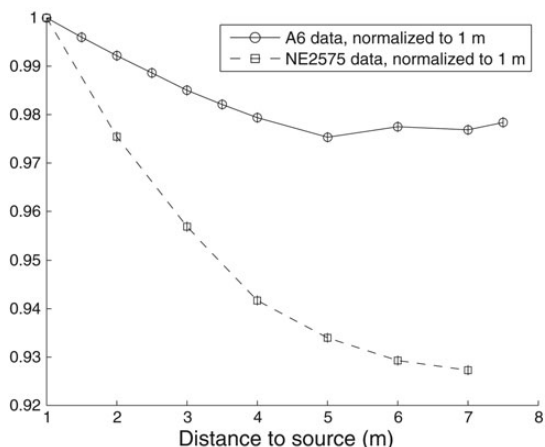


Figure 5. Raw data, inverse-square corrected, for the A6 and NE2575 instruments.

Table 1. Factors contributing to the inverse-square anomaly.

#	Contributing cause	Change
1	Attenuation of primary gamma rays in the air between the source and the instrument	-
2	Generation of scattered gamma rays in the air between and around the source and detector, including the physical enclosure of the laboratory (floor, walls, ceiling)	+
3	Systematic error in detector alignment and a systematic error in placing the centre of the sensitive volume of the detector at the assumed distance from the source	±
4	Primary gamma-ray attenuation in the material of the detector itself	-
5	Generation of scattered gamma rays in the material of the detector	+
6	Electron drift of those electrons that generate ions in the chamber gas, that arise upstream, on average, from the chamber centre <sup>a</sup>	+
7	Electron angular distributions <sup>b</sup>	+
8	Ion collection efficiency	+

<sup>a</sup>Discussed in ref. (3).

<sup>b</sup>Discussed in ref. (4).

The NE2575 exhibits a much more dramatic decrease. Explaining this behaviour is what motivated the current study.

## ANALYSIS

### Accounting for attenuation in the air

The A6, being spherical in shape, has very well established inverse-square stability<sup>(4, 5)</sup>. Its decrease for distances less than  $\sim 4$  m is consistent with the exponential attenuation in the intervening air. Therefore, this chamber may be used to eliminate the air attenuation. Moreover, the room scatter may also be mostly eliminated from the NE2575 by dividing the NE2575 readings by the A6 readings, thereby approximating the readings that would be obtained, in vacuum, by the NE2575 alone. Small discrepancies from the differential absorption of photons, by the thick rear wall of the NE 2575, may persist, but they are believed to be small. The result is shown in Figure 6.

This accounts for causes 1 and 2 in Table 1. Careful experimental technique can minimise causes 3 and 8, while causes 6 and 7 are known to be small, leaving only causes 4 and 5 as possible sources of the anomaly.

### Is the anomaly caused by room scatter?

The NE2575 has a thick 1.5 cm rear wall, downstream from the source. A measurable amount of photon scatter must arise from this rear wall. However, the rear wall of the chamber also shields the chamber from photons that have backscattered from the back wall of the low-scatter laboratory.

It is known that a planar surface source has a logarithmically divergent particle fluence in the vicinity of its surface. Therefore, it was hypothesised that the shielding by the thick rear wall of the NE2575 would

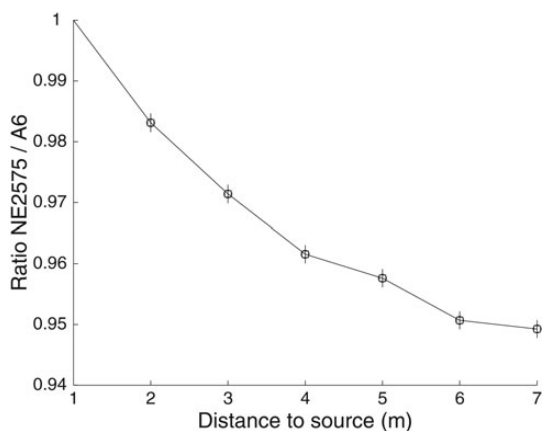


Figure 6. Ratio of the NE2575 to the A6, removing the effect of attenuation in the air and room scatter.

lead to a reduction in measured ionisation, compared with the thin-walled A6.

To study this, the data of the A6 were revisited, but corrected for attenuation from the small distance data. The results are shown in Figure 7. The dashed line presents a simple analytic method that models the scatter from the walls of the laboratory.

The deviation from the model is likely the result of the geometry of the room, since the low-mass floor and pit, which end at  $\sim 8$  m from the source, generate less scatter at the measurement point (see Figure 2).

These data in Figure 7 show that room scatter, and the shielding from its rear wall, is not the explanation. This effect accounts for only a few tenths of a per cent at 4 m. The principal cause of the anomaly was revealed by Monte Carlo modelling of the two chambers.

## MONTE CARLO CALCULATIONS

Monte Carlo calculations were employed to confirm whether the chamber itself—and which parts therein—are responsible for the observed anomalous behaviour. The EGSnc simulation package<sup>(6)</sup> that has been adapted for 30 y for low-energy electron transport<sup>(7)</sup> was used, with the accurate calculation of ionisation chamber response as a central application theme<sup>(8–10)</sup>. This code system is able to resolve relative differences between two chambers at the 0.1 % level, and is ideal for investigating the response of the NE2575 relative to the A6. Absolute comparisons require accurate knowledge of the fundamental cross sections, and this is much more uncertain.

Realistic models of the chambers using the egs++ geometry library were built, as shown in Figures 8 and 9. The A6 was modelled as a 0.3 cm-thick, air-filled

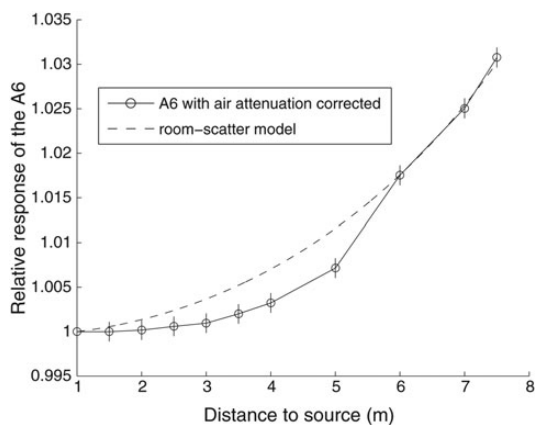


Figure 7. The solid line represents the A6 data, corrected for primary photon attenuation. The dashed line is a theoretical prediction for the scatter component from the walls of the low-scatter laboratory.

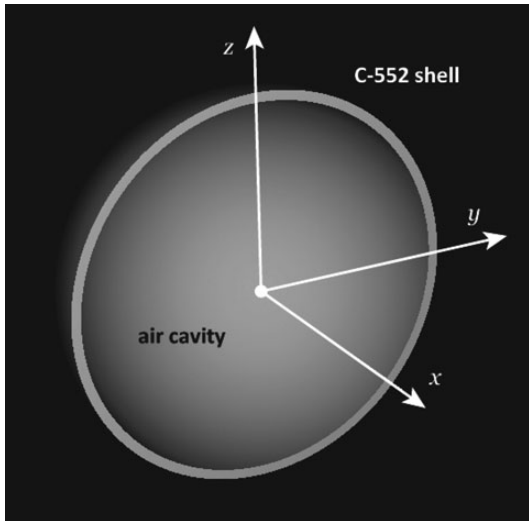


Figure 8. The EGSnrc model of the A6: a 0.3-cm thick C-552 plastic shell enclosing a 5.72 cm radius air cavity. The A6 central electrode was not modelled. In the simulation set-up, the isotropic point source was located on the negative  $z$ -axis, from  $z = -0.2$  m to  $z = -8$  m. The dose was collected in the air cavity.

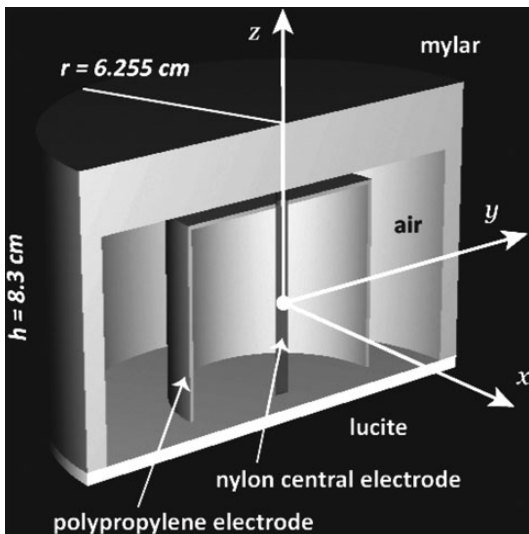


Figure 9. The EGSnrc model of the NE2575: overall dimensions and materials of the chamber are shown. All other dimensions are as indicated on original technical drawings or as measured on the chamber itself. In the simulation set-up, the isotropic point source was located on the negative  $z$ -axis, from  $z = -0.2$  m to  $z = -8$  m. Hence, most photons would enter the chamber through the Lucite front wall and exit via the thick rear wall. The dose is collected in the air cavity.

C-552 plastic shell with an internal radius of 5.72 cm (the central electrode was not modelled). The dimensions of the NE2575 that were employed were based on technical drawings and direct measurements of the disassembled chamber. The compositions and densities of materials employed were from the standard database distributed with EGSnrc. In the model, Mylar was used for the NE2575 side wall and rear wall, instead of SRBP, since Mylar has similar chemical components and density.

The simulation environment consisted of a  $2 \times 2 \times 11$  m<sup>2</sup> cuboid filled with air, centred on the negative  $z$ -axis at  $z = -4.5$ , which encompasses the source and the detectors with at least 1 m of air buffer. Both chambers were positioned so that the centres of their air cavities were located at the origin. A spectrum point source of <sup>137</sup>Cs was placed on the chamber axis, at various distances from the chamber along the negative  $z$ -axis, in order to reproduce measurements as a function of distance. The source was isotropic but, for the sake of simulation efficiency, was numerically collimated to a circular field with a radius of 10 cm at the chamber location, viz. the  $d$  parameter used in this paper. It was verified that using a realistic model of the <sup>137</sup>Cs source capsule or increasing the collimation angle did not affect the results obtained here (data not shown).

Global kinetic energy cut-offs of 10 keV for both electrons and photons were chosen, with all advanced physics options turned on and all variance reduction techniques turned off. Under these conditions, data points typically each require 150 CPU-hours to reach statistical uncertainties on the order of 0.01 % (using  $10^{11}$  histories). It was verified that using smaller transport cut-offs of 1 keV for electrons and photons did not affect the results obtained here (data not shown).

The custom `egs++` application transported particle showers generated from the <sup>137</sup>Cs source photons through the A6 and NE2575 simulation geometries, and reported the dose to the air cavity of each chamber. In addition, the code also reported dose components for the NE2575, i.e. the contributions to the total cavity dose from different parts of the chamber. This was accomplished by tallying the dose according to the chamber component in which the particle (or its ancestors in the particle shower) last underwent a discrete interaction. Thus, one kept track of dose contributions from the front wall, the side wall, the rear wall, the electrode and the air cavity itself.

Figure 10 is plotted the relative deviation in dose for the NE2575, compared with the A6. The data are normalised at 1 m. Denoting by  $\hat{D}$  the dose relative to that deposited in the A6, this graph shows, for the whole chamber and each chamber component  $i$ , as labelled, the quantity  $[\hat{D}_i(d) - \hat{D}_i(d_0)] / \hat{D}_{NE2575}(d_0)$ , with  $d_0 = 1$  m. The contributions of individual components sum up to that of the whole chamber.

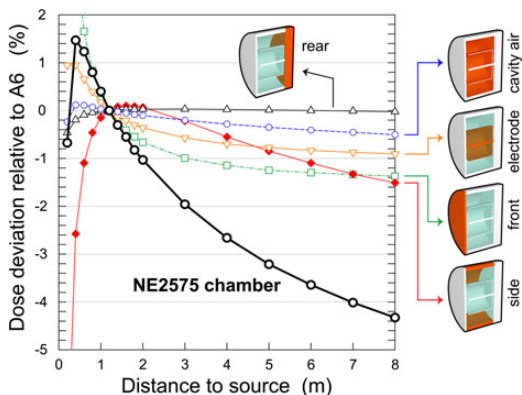


Figure 10. Relative dose deviation relative to the A6, as calculated by Monte Carlo. Statistical uncertainties in all cases are smaller than the data point symbol. The thick solid line shows the relative dose deviation for the whole NE2575, and the other curves show the contributions to the total deviation from each chamber component, as indicated.

The data in Figure 10 suggest that the Monte Carlo modelled NE2575/A6 ratio is  $-4.0\%$  compared with the measured ratio of  $-5.0\%$  seen in Figure 6. It would appear that this discrepancy is consistent with an incomplete simulation model of the scatter radiation of the room, further suggested by Figure 7. At 7 m, that scatter component from the laboratory enclosure is  $\sim 2.3\%$ . That the measured NE2575/A6 deficit is greater than the calculated one is consistent with a less energetic scatter component from the room.

Nonetheless, the Monte Carlo results are most informative. All chamber components, except the thick rear wall, contribute to the deficit. At 7 m the relative contributions are:  $-1.4\%$  for both the front wall and the side wall,  $-0.8\%$  for the electrode and  $-0.4\%$  for the cavity air.

It is interesting to note the different distance behaviours of the various chamber components. Even at 7 m from the source, the side wall has not yet approached its asymptotic, large-distance value. It is known that this behaviour has a large first-order (length of wall/distance to source) nature. The front wall and rear wall, whose behaviour is known to be second order, have nearly reached their asymptotic values. The cavity air and the electrode have intermediate behaviours.

#### PHENOMENOLOGICAL METHOD TO CORRECT FOR THE ANOMALY

The observations made in the previous paragraph, and a recent paper on the large-distance behaviour of ionisation chambers in photon beams<sup>(2)</sup>, suggest an alternative approach to characterise the inverse-square anomaly of the NE2575 and the A6. Even at the

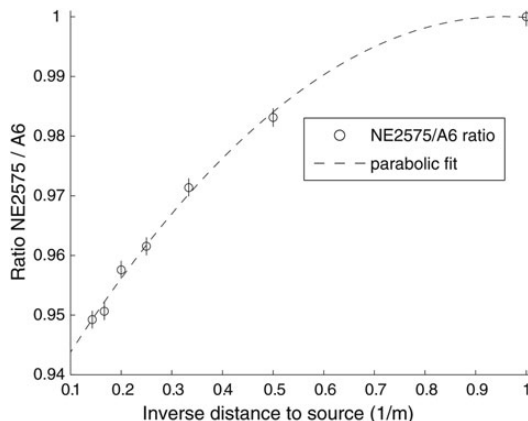


Figure 11. The response ratio vs.  $1/d$ .

closest measurement distance, all dimensions of these chambers are much less than the source–detector distance. Therefore, an expansion of the form

$$M_{A6}^{NE2575}(d) = p_0 + \frac{p_1}{d} + \frac{p_2}{d^2} \dots \quad (1)$$

where  $d$  is the source–detector distance, is proposed as a phenomenological/empirical model to describe the NE2575/A6 ratio,  $M_{A6}^{NE2575}(d)$ . The fitting constants  $p_i$  have dimensions  $(\text{length})^i$ .

The parameters have physical interpretation associated with them. Here  $p_0$  is the extrapolated ratio as  $d \rightarrow \infty$ . One finds  $\sum_i p_i/d_0^i$ , where  $d_0$  is the normalisation point (1 m in this case) and should be close to unity, if the hypothesis is true. In this case, the fitting parameters obtained were:  $p_0 = 0.9299$ ,  $p_1/d_0 = 0.1465$  and  $p_2/d_0^2 = -0.0765$ ,  $1 - \sum_i p_i/d_0^i = 1.1 \times 10^{-4}$ , the latter datum giving a measure of the goodness of fit.

Further support for this hypothesis is given in Figure 11, which plots the data in terms of the response ratio vs.  $1/d$ . The parabolic three-parameter fit, shown as a dashed line, fits the empirical data adequately.

Figure 12 shows the result of applying the parabolic correction to the data, which appears to explain the anomaly, at least in a phenomenological fashion.

The fitting constants obtained herein, are specific to this study, and should not be adopted universally. It would be possible to provide universal constants for the NE2575 alone, or indeed, any measurement device. Using standard collimation and standard sources, and employing the assumption of an unbounded air-filled laboratory, those fitting constants (calculated by Monte Carlo methods) would also account completely for the attenuation of primary photons in the air, and to some extent for the small signal obtained from scattered photons from the air. The only installation-specific difference would be the geometry of the

## INVERSE-SQUARE ANOMALY OF THE NE2575 ION CHAMBER

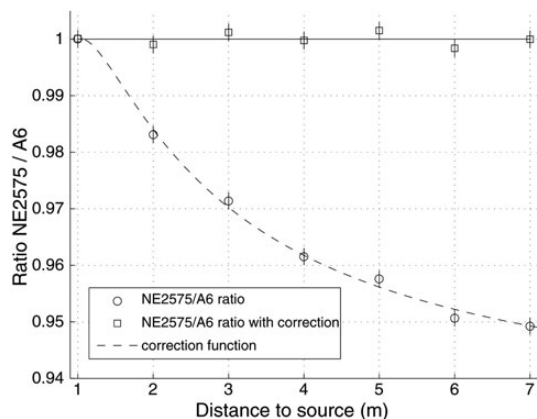


Figure 12. The NE2575/A6 ratio, and the parabolic correction.

room, which would cause differing scattering characteristics.

### CONCLUSION

The inverse-square anomaly has been resolved, explained by photon attenuation in the walls, electrodes and cavity air. These components have attenuation path-lengths that vary significantly during the course of an inverse-square consistency check. A phenomenological/empirical correction has been proposed that appears to resolve the inconsistency. While the results of the proposed correction are convincing, an *ab initio* theory, which corroborates the phenomenological theory, would be welcome.

### ACKNOWLEDGEMENTS

The hospitality of the Ionizing Radiation Standards Group, at the National Research Council of Canada, Ottawa, is gratefully acknowledged. Part of this work was performed there, during a sabbatical leave. The lively discussion with Ernesto Mainegra-Hing, Malcolm

McEwen, Carl Ross, Brad Downton (who did some of the preliminary measurements), and Blake Walters (who did some of the preliminary Monte Carlo calculations) is greatly appreciated. Special mention is due to Pete Burgess, formerly of Nuvia Limited (UK), for many discussions, and his support during the execution of this work.

### REFERENCES

- Shortt, K. R., Ross, C. K. and Janovsk?, I. *The response of LIF TLDS to  $^{137}\text{Cs}$  and  $^{60}\text{Co}$   $\gamma$  rays.* Radiat. Prot. Dosim. **69**, 257–266 (1997).
- Bielajew, A. F. *Minimizing the  $1/r^2$  perturbation for ideal fluence detectors in small source  $\gamma$ -irradiation fields.* Phys. Med. Biol. **59**, 4465–4475 (2014).
- Bielajew, A. F. *Ionization cavity theory: a formal derivation of perturbation factors for thick-walled ion chambers in photon beams.* Phys. Med. Biol. **31**, 161–170 (1986).
- Bielajew, A. F. *An analytic theory of the point-source non-uniformity correction factor for thick-walled ionisation chambers in photon beams.* Phys. Med. Biol. **35**, 517–538 (1990).
- Kondo, S. and Randolph, M. L. *Effect of finite size of ionization chambers on measurements of small photon sources.* Radiat. Res. **13**, 37–60 (1960).
- Kawrakow, I., Mainegra-Hing, E., Rogers, D. W. O., Tessier, F. and Walters, B. R. B. *The EGSnrc Code System: Monte Carlo simulation of electron and photon transport.* Technical Report PIRS–701, National Research Council of Canada (2013).
- Rogers, D. W. O. *Low energy electron transport with EGS.* Nucl. Instrum. Methods **227**, 535–548 (1984).
- Bielajew, A. F., Rogers, D. W. O. and Nahum, A. E. *Monte Carlo simulation of ion chamber response to  $^{60}\text{Co}$ —resolution of anomalies associated with interfaces.* Phys. Med. Biol. **30**, 419–428 (1985).
- Kawrakow, I. *Accurate condensed history Monte Carlo simulation of electron transport, Part I: EGSnrc, the new EGS4 version.* Med. Phys. **27**, 485–498 (2000).
- Kawrakow, I. *Accurate condensed history Monte Carlo simulation of electron transport, Part II: application to ion chamber response simulations.* Med. Phys. **27**, 499–513 (2000).